One-Plane Glide-Symmetric Structures Over Dielectric Substrate

A. Tamayo-Domínguez[1*], J.M. Fernández-González[1] and O. Quevedo-Teruel[2]

[1]Department of Signals, Systems and Radiocommunications, Universidad Politécnica de Madrid, 28040, Madrid, Spain.
[2]Division of Electromagnetic Engineering, KTH Royal Institute of Technology, Stockholm 10044, Sweden.
a.tamayo@upm.es; jmfdez@gr.ssr.upm.es; oscarqt@kth.se. [1*]ORCID: orcid.org/0000-0002-2322-3800

***Abstract*—This work presents a new configuration to create glide-symmetric structures in a single plane, which can be printed on the metallic face of a dielectric substrate. This type of glide symmetry facilitates the fabrication and avoids alignment problems in the assembly process when compared to traditional glide-symmetric structures based on several planes. This article also includes a study based on dispersion diagrams on the appearance of stop-bands by breaking the symmetry. Finally, we present the simulated S parameters of structures with 10x10 unit cells to illustrate the attenuation in these stop-bands.**

***Index Terms*— glide symmetry, single-plane, stop-band, periodic structures, higher symmetries.**

I. Introduction

THE growing interest in the use of periodic structures to improve the electromagnetic properties of antennas and microwave devices has been a major driving force in the recent study of higher symmetries [1][2]. These symmetries were first investigated in the 60s and 70s for one-dimensional periodic structures [3][4]. However, it has been more recently when two-dimensional glide symmetries, which are a particular case of higher symmetries, have been proposed and studied, demonstrating a great potential to modify the dispersion properties of periodic structures. Periodic glide-symmetric structures are obtained by a reflection and a translation of a unit cell. Glide symmetries have been successfully used to reduce the dispersion of periodic structures [5-7], or to increase the width and attenuation of electromagnetic bandgaps [8-11]. For example, glide symmetry has been proposed to produce lens antennas for 5G communications [12][13] taking advantage of their ability to produce higher refractive index, less dispersion and more isotropy [14]. Prior to this work, all the glide-symmetric structures proposed in the literature for parallel plate configurations have a horizontal plane of symmetry, perpendicular to the direction of propagation. These configurations need of two different planes, which increases the complexity of manufacturing and may introduce alignment problems.

In this paper, we propose a glide-symmetric structure in a single plane with ellipses printed on a dielectric substrate as a basic element. Glide symmetry is achieved by locating the plane of symmetry vertically rather than horizontally, preserving the orthogonality to the direction of propagation. The propagation is an air gap above the plane of the ellipses, so the structure has low losses. The use of a dielectric substrate instead of a fully-metallic structure allows the introduction of additional degrees of freedom, including the ability to modify or break the glide symmetry in the case of using a substrate that may have different dielectric constant values (e. g. liquid crystals [15]). The orientation, size and position of these ellipses will determine the electromagnetic properties of the structure in terms of dispersion, stop-bands or refractive index.

This paper is organized in five sections. The section II shows the basic properties and parameters of the glide-symmetric unit cell and some operation examples. Section III presents the possibility of regenerating the glide symmetry from a symmetry-broken structure maintaining the value of all parameters. In section IV, the performance of these new structures is illustrated with the S-parameters of a full design with 10x10 unit cells. Finally, in section V, conclusions are drawn.

II. Parameters and Basic Operation of the Unit Cell

The presented structure consists of two different layers. The lower layer is a plated dielectric substrate sheet in which the metal corresponding to the elliptical glide-symmetric shapes is removed in one of the faces. The top layer is a metal plate separated a certain distance from the dielectric substrate, which generates an air gap where the fields can or cannot propagate. The Fig. 1 represents all the parameters that can be modified to vary the behaviour of the dispersion diagram of the unit cell. Fig. 1(a) shows the air h_{Air} and dielectric substrate h_{Diel} thicknesses, together with the dielectric constant ε_{r} of the substrate and the period p. It should be noted that the calculations of the dispersion diagrams have been made considering periodic conditions in x and y directions. Thus, in the direction of propagation y the structure has two periodicities, whereas in the perpendicular x direction it has only one. Fig. 1(b) depicts the parameters relative to the size, position, orientation and shape of the ellipses, which will determine the basic behaviour of the complete structure. Specifically, the size of the major and minor semi-axes of the ellipses is defined by the values of A_1 and B_1 for the first ellipse and A_2 and B_2 for the second one. The angle of inclination is defined in degrees by the parameters φ and θ for the first and second ellipses. The rotation is counter-clockwise for the first ellipse and clockwise for the second ellipse, starting from the horizontal position. Finally, the displacement parameter d

indicates the distance of the second ellipse from the first ellipse. A zero value of this parameter means that the distance is maintained under glide symmetry conditions, that is a distance p between ellipses centres, while values greater than zero indicate that the second ellipse is shifted towards the first ellipse.

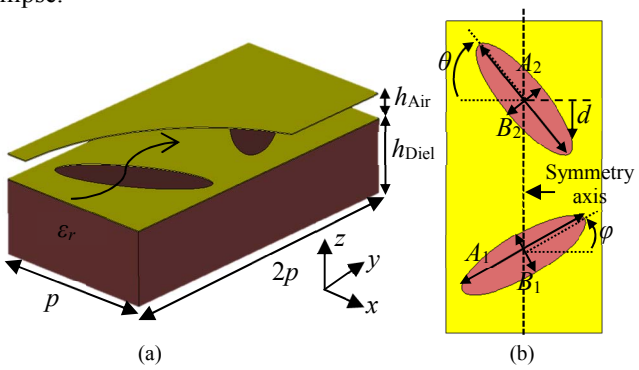

Fig. 1. Unit cell of the proposed structure and parametrization. View in perspective (a) and top view without the top metal plate (b).

Given the definition of the structure parameters in Fig. 1, it is observed that the glide-symmetric configuration is achieved when $A_1 = A_2$, $B_1 = B_2$, $\varphi = \theta$ and $d = 0$. The axis of symmetry in this case is at the centre of the structure along the y direction and the glide symmetry is obtained by mirroring the initial ellipse through the axis of symmetry and displacing the ellipse obtained a distance p in the y direction. An example of how glide symmetry operates is illustrated in Fig. 3 (a-c), which depicts the dispersion diagrams of the structures shown in Fig. 2 (a-c). The results have been obtained using the Eigenmode solver in *CST Microwave Studio*. Only phase variations in y direction are represented in the dispersion diagrams that is the direction of interest. The chosen parameters in Fig. 2(a) are: $\varepsilon_r = 3$, $h_{Air} = 0.2$ mm, $h_{Diel} = 1.52$ mm, $p = 3.3$ mm, $A_1 = A_2 = 3$ mm, $B_1 = B_2 = 0.9$ mm and $d = 0$ mm. The only difference between unit cells in Fig. 2(a), Fig. 2(b) and Fig. 2(c) is the value of angles φ and θ. Fig. 2(a) is a glide-symmetric structure with $\varphi = \theta = 30°$. This symmetry is slightly broken by changing θ to 90° in Fig. 2(a) and maximally broken in Fig. 2(c) by changing both φ and θ to 0° and 90°.

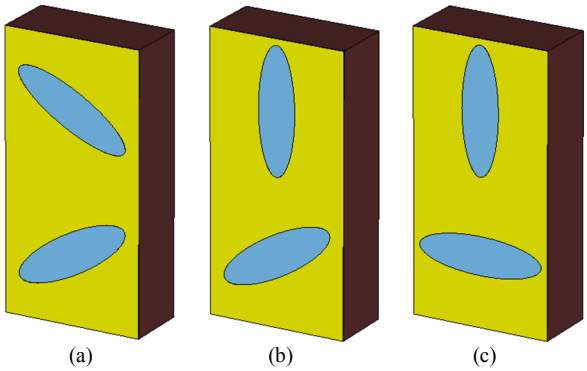

Fig. 2. Unit cell of a glide-symmetric (a), non-glide-symmetric (b) and maximally non-glide-symmetric (c) structures.

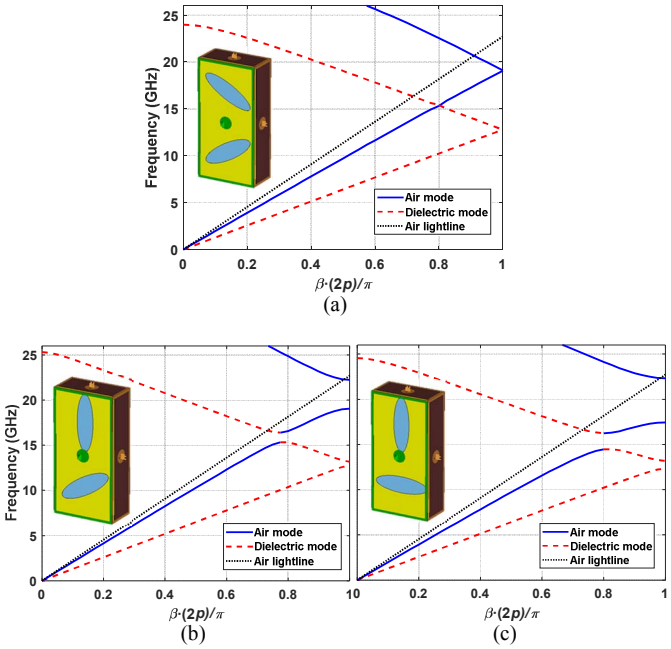

Fig. 3. Dispersion diagrams for three configurations of the unit cell: glide-symmetric (a), non-glide-symmetric (b) and maximally non-glide-symmetric (c).

In the dispersion diagrams shown in Fig. 3, there are two modes that correspond to the modes that propagate inside the dielectric substrate and through the air gap. The mode of interest in this case is the one that propagates in the air, since it has lower losses. As expected in a parallel plate propagation, non-dispersive modes are obtained up to certain frequencies for the glide-symmetric case (Fig. 2(a)). However, the immediate effect of breaking symmetry (Fig. 2(b-c)) is the appearance of stop-bands or frequency ranges in which the fields do not propagate in the chosen direction. This effect occurs both in the dielectric and air mode, although the stop-band width is much larger in the second case. This is because the air gap is thinner than the dielectric one and the field is more confined, so the ellipse effect is greater in the air mode. It is observed that the symmetry rupture generates a stop-band on the right side of the dispersion diagram, as expected from a periodic glide-symmetric structure with two periodicities [8]. This stop-band is wider when the symmetry is maximally broken (Fig. 3 (c)), which goes from 17.44 GHz to 22.33 GHz, while the stop-band range is 19.07 GHz to 22.25 GHz in Fig. 3(b). Another interesting effect on these structures is the appearance of an additional stop-band produced by the merging of the forward mode in the air with the backward mode in the dielectric. This kind of stop-band was explained in [16] as a complex mode propagating in the structure.

III. Regenerating the Glide Symmetry

An interesting property of the structures analyzed in this work is that to regenerate the glide symmetry from a structure with the symmetry broken is possible. The procedure is similar to the one explained for the unit cells studied in section II, but instead of using the center of the structure as the center of symmetry, we use one of the lateral edges. Fig. 4 shows that after mirroring and translating the structure a distance p in the

direction of propagation, a glide-symmetric unit cell is obtained again. Of special interest is the case in which the unit cell with broken symmetry has mirror symmetry, that is, it is identical to the mirrored unit cell considering the center of the unit cell in direction *y* as axis of symmetry. This is the case of the unit cell in Fig 2(c) and the one used in Fig. 4. This situation allows to design reconfigurable structures based on the relative displacement of alternate rows in the direction of propagation, which allows to obtain a structure with reconfigurable stop-band breaking and regenerate the glide symmetry.

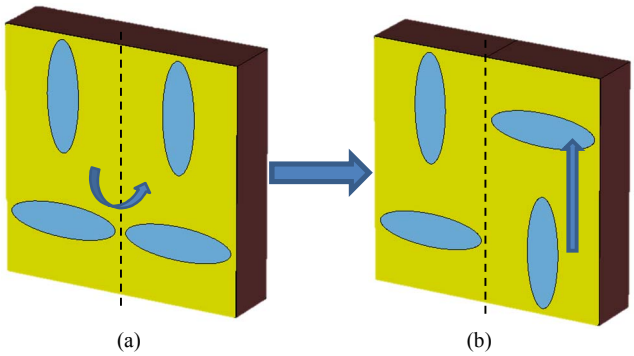

Fig. 4. The non-glide-symmetric structure in Fig. 2 (c) mirrored using a different symmetry axis (a). The new glide-symmetric structure (b) is obtained from (a) after applying a translation.

The dispersion diagram of the new glide-symmetric unit cell in Fig. 4 (b) is shown in Fig. 5, together with the dispersion diagram of the original structure (Fig. 2(c)) for comparison. It is observed that all stop-bands are closed completely, so the propagation in the whole analyzed frequency band is recovered.

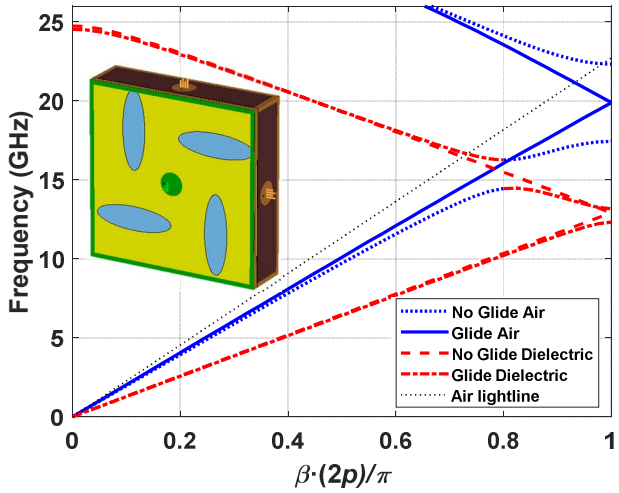

Fig. 5. Dispersion diagram of the structure in Fig. 4(b) with regenerated symmetry compared to the original non-glide-symmetric structure in Fig. 2(c).

IV. Simulations and Final Results

To finish the study of the structures presented in Fig. 2 and Fig. 4, we have built four complete models to excite with waveguide ports and obtained the S parameters. The first three models (Fig. 6 (a-c)) contain 10x10 of the unit cells illustrated in Fig. 2 (a-c). The fourth model in Fig. 6 (d) consists of only 5x10 unit cells from the structure in Fig. 4 (b), as it is twice as wide as the others. Then, the total size is 33x66 mm. The ports excite only the air gap above the metal ellipses with a TE_{10} mode. For the simulations, the losses in metals and dielectrics have been considered, using copper (σ=5.8·10^7) as metal, and a loss tangent *td*=0.0035 for the dielectric substrate. The ports are electrically shielded and consider the first four modes. The boundaries in the structures are electrical (E_t=0) in *x* and *z* directions and open in the *y* direction.

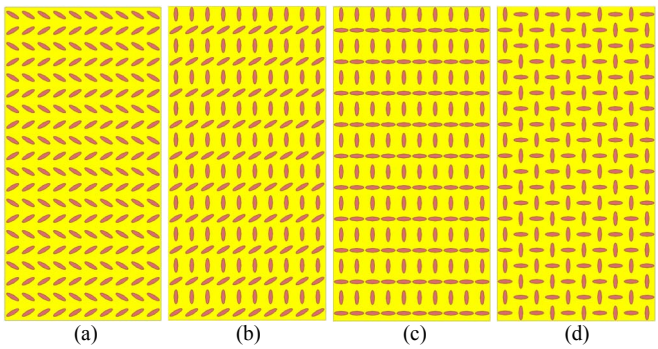

Fig. 6. Full designs with 10x10 unit cells of a glide-symmetric (a), non-glide-symmetric (b) and maximally non-glide-symmetric (c) structures and 5x10 unit cells of the regenerated glide-symmetric design (d).

The results obtained in simulation are presented in three subsections. In subsection IV A, the effect of the rupture of the symmetry on the S parameters is shown. In subsection IV B, the results of the regeneration of the symmetry are represented. Finally, the comparison of the absolute value of the electric field inside the four structures of Fig. 6 is carried out in subsection IV C for different frequencies.

A. Breaking the symmetry

In Fig. 7(a), the parameter S_{21} for structures in Fig 6 (a-c) is depicted together with the modes in air of the dispersion diagrams in Fig. 3. Parameter S_{11} is shown in Fig. 7(b).

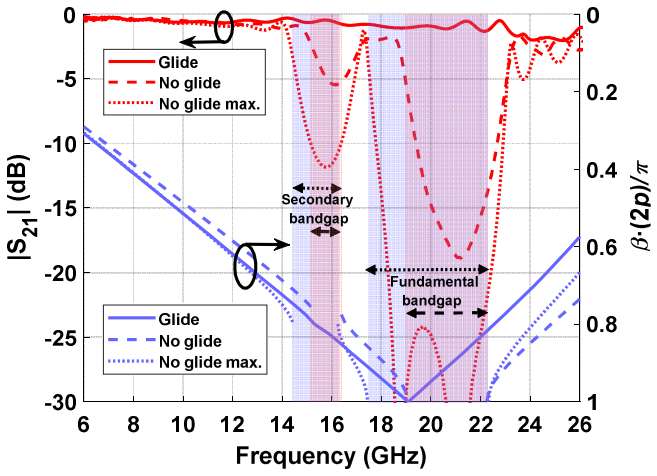

(a)

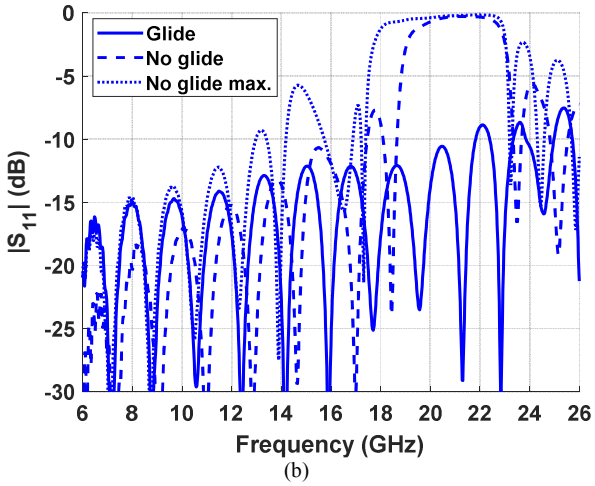

(b)

Fig. 7. Simulated S parameters of the designs in Fig. 6 (a-c). The S_{21} parameters are shown together with the dispersion diagrams to compare the position of the stop-bands (a). The S_{11} parameters are shown in (b).

The stop-bands increase when the symmetry rupture is greater, as already observed in the dispersion diagrams in Fig. 3. However, the S parameters in Fig. 7 show that not only does the frequency range of the stop-bands increases, but also the attenuation of the field at the output. First, we focus on the fundamental stop-band as the secondary stop-band produced by the merging of the forward and backward modes in air and in dielectric works differently. In Fig. 7(a), the S_{21} parameter in the glide configuration (solid line) is around -1 or -2 dB, but this value falls below -15 dB for the case of partial symmetry rupture (dashed line) and reaches values below -25 dB for a maximum symmetry rupture (dotted line). The representation of parameter S_{11} in Fig. 7(b) shows that this attenuation at the output occurs because most of the power is reflected towards the input. However, this is not the case with the secondary stop-band, whose output attenuation levels are -5 and -10 dB for the cases of partial rupture and maximum rupture. Therefore, this missing power must be injected into the dielectric, as it is not reflected towards the input. An additional detail observed in Fig. 7(a) is that the attenuation produced by the stop-bands does not appear centered with respect to the stop-bands obtained in the dispersion diagrams. The reason for this is that the simulated structures are not infinitely periodic and the propagated modes within them have a low but not zero cut-off frequency. This condition results in the small shift upward in frequency observed in the simulations.

B. Regenerating the symmetry

For a better visualization of the symmetry regeneration, Fig. 8 shows a comparison of parameter S_{21} (Fig. 8(a)) and S_{11} (Fig. 8(b)) of the regenerated symmetry design (solid line), the original design with maximum symmetry rupture (dashed line) and the original glide-symmetric design (dotted line). The stop-bands disappear completely and the initial broadband transmission is recovered with attenuation values around -1 or -2 dB.

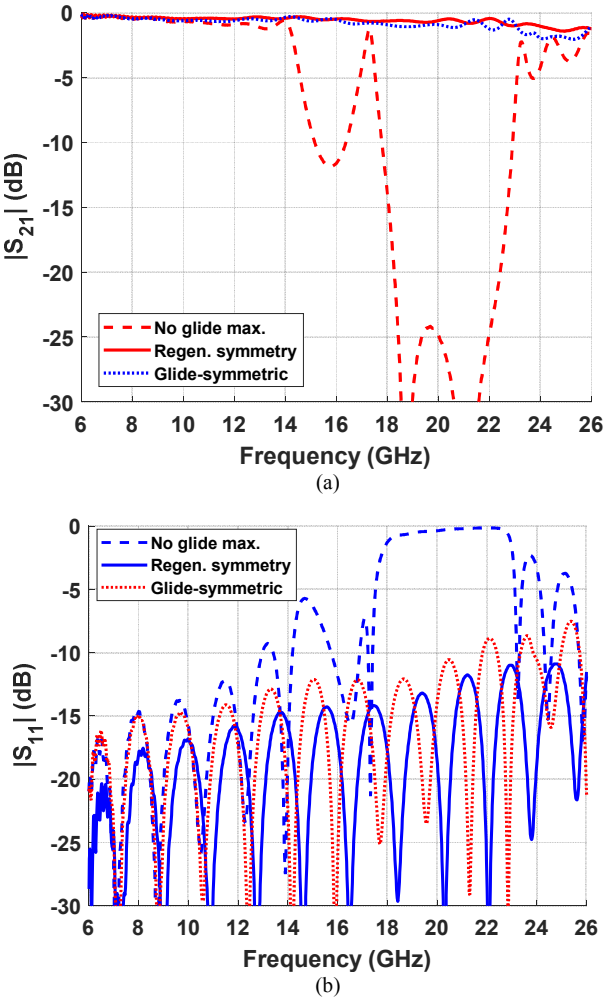

Fig. 8. Simulated S parameters of the design with regenerated symmetry in Fig. 6 (d) compared to the results of the original glide and non-glide designs. The S_{21} parameters are shown in (a) and the S_{11} parameters are shown in (b).

C. Electric fields

Finally, this subsection represents in Fig. 9 the electric field monitors in the four structures of Fig. 6 for six selected frequencies.

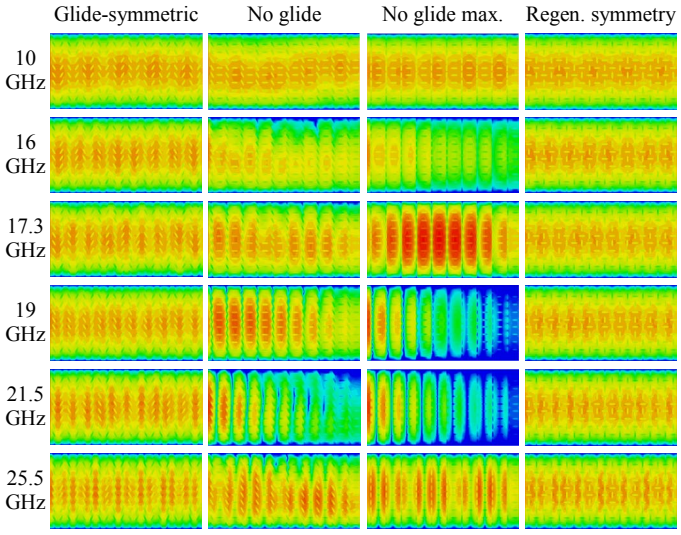

Fig. 9. E-fields of structures in Fig. 6 at 10, 16, 17.3, 19, 21.5 and 25.5 GHz.

Fig. 9 presents a comparison of the behavior of the electric field inside the air gap, specifically in a cut at half the height of the gap. The selected frequencies aim to collect the outstanding phenomena in the analysis of these structures, including: propagation at frequencies below the two stop-bands (10 GHz), the field at the maximum attenuation at the secondary stop-band (16 GHz), propagation at the frequencies between the two stop-bands (17.3 GHz), the beginning of the fundamental stop-band in the design with the symmetry partially broken together with a stop-band in full operation of the design with maximum rupture of the symmetry (19 GHz), maximum attenuation of the fundamental stop-band (21.5 GHz) and propagation at a frequency above the two stop-bands (25.5 GHz). Both the original glide-symmetric and regenerated designs present a homogeneous electric field distribution along the structure for all chosen frequencies. It is noteworthy the difference in attenuation of the designs with rupture of the symmetry, in which the electric field level is progressively reduced along the structure.

V. Conclusion

A new type of glide symmetry based on a single plane has been introduced in this work. The analysis of dispersion diagrams and S parameters of structures conserving or breaking this new symmetry has demonstrated the utility of these structures to generate stop-bands and different levels of attenuation. The implementation is done using ellipses with a certain orientation on the metallic face of a dielectric substrate. Unlike the previous glide-symmetric structures described in the literature, the alignment of this surface with an upper metal plate to generate the necessary air gap is not a problem when manufacturing a prototype based on this technology. The results show an attenuated band of 25 % centred on approximately 20 GHz with an attenuation level of around 25 dB in a total length of 66 mm. Finally, the ability of mechanical reconfigurability of a design to break or regenerate the glide symmetry has been demonstrated.

Acknowledgment

Simulations done in this work have been performed using CST Microwave Studio Suite 2018 under a cooperation agreement with Computer Simulation Technology (CST). Authors would like to acknowledge the Spanish Government, Ministry of Economy, National Program of Research, Development and Innovation for the support of this publication in the projects ENABLING-5G “ENABLING INNOVATIVE RADIO TECHNOLOGIES FOR 5G NETWORKS” (project number TEC2014-55735-C3-1-R), FUTURE-RADIO "Radio systems and technologies for high capacity terrestrial and satellite communications in an hyperconnected world" (project number TEC2017-85529-C3-1-R) and the Madrid Regional Government under the project SPADERADAR “Space Debris Radar” (S2013/ICE-3000).

References

[1] F. Ghasemifard, M. Norgren and O. Quevedo-Teruel, "Dispersion Analysis of 2-D Glide-Symmetric Corrugated Metasurfaces Using Mode-Matching Technique," in *IEEE Microwave and Wireless Components Letters*, vol. 28, no. 1, pp. 1-3, Jan. 2018.

[2] G. Valerio, F. Ghasemifard, Z. Sipus, O. Quevedo-Teruel, “Glide-Symmetric All-Metal Holey Metasurfaces for Low-Dispersive Artificial Materials: Modeling and Properties", *IEEE Transactions on Microwave Theory and Techniques*, vol. 66, no. 7, pp. 3210-3223, July 2018.

[3] P. J. Crepeau and P. R. McIsaac, "Consequences of symmetry in periodic structures," in *Proceedings of the IEEE*, vol. 52, no. 1, pp. 33-43, Jan. 1964.

[4] A. Hessel, Ming Hui Chen, R. C. M. Li and A. A. Oliner, "Propagation in periodically loaded waveguides with higher symmetries," in *Proceedings of the IEEE*, vol. 61, no. 2, pp. 183-195, Feb. 1973.

[5] M. Camacho, R. C. Mitchell-Thomas, A. P. Hibbins, J. R. Sambles, O. Quevedo-Teruel, “Designer surface plasmon dispersion on a one-dimensional periodic slot metasurface with glide symmetry”, *Optics Letters*, Vol. 42, No. 17, pp: 3375-3378, 2017.

[6] M. Camacho, R.C. Mitchell-Thomas, A.P. Hibbins, J.R. Sambles and O. Quevedo-Teruel, "Mimicking glide symmetry dispersion with coupled slot metasurfaces," in *Applied Physics Letters*, vol. 111, no 12, p. 121603, 2017.

[7] P. Padilla, L. F. Herran, A. Tamayo-Dominguez, J. F. Valenzuela-Valdes, O. Quevedo-Teruel, "Glide Symmetry to Prevent the Lowest Stopband of Printed Corrugated Transmission Lines", *IEEE Microwave and Wireless Components Letters*, vol. 28, no. 9, pp. 750-752, Sept. 2018.

[8] M. Ebrahimpouri, O. Quevedo-Teruel and E. Rajo-Iglesias, "Design Guidelines for Gap Waveguide Technology Based on Glide-Symmetric Holey Structures," in *IEEE Microwave and Wireless Components Letters*, vol. 27, no. 6, pp. 542-544, June 2017.

[9] M. Ebrahimpouri, E. Rajo-Iglesias, Z. Sipus, O. Quevedo-Teruel, "Cost-Effective Gap Waveguide Technology Based on Glide-Symmetric Holey EBG Structures”, *IEEE Transactions on Microwave Theory and Techniques*, vol. 66, no. 2, pp. 927-934, Feb. 2018.

[10] M. Ebrahimpouri, A. Algaba-Brazalez, L. Manholm, O. Quevedo-Teruel, "Using Glide-symmetric Holes to Reduce Leakage between Waveguide Flanges", *IEEE Microwave and Wireless Components Letters*, vol. 28, no. 6, pp. 473-475, June 2018.

[11] E. Rajo-Iglesias, M. Ebrahimpouri, O. Quevedo-Teruel, “Wideband phase shifter in groove gap waveguide technology implemented with glide-symmetric holey EBG”, *IEEE Microwave and Wireless Components Letters*, vol. 28, no. 6, pp. 476-478, June 2018.

[12] O. Quevedo-Teruel, J. Miao, M. Mattsson, A. Algaba-Brazalez, M. Johansson, L. Manholm, "Glide-symmetric fully-metallic Luneburg lens for 5G Communications at Ka-band", *IEEE Antennas and Wireless Propagation Letters*, vol. 17, no. 9, pp. 1588-1592, Sept. 2018.

[13] O. Quevedo-Teruel, M. Ebrahimpouri, F. Ghasemifard, “Lens Antennas for 5G Communications Systems”, *IEEE Communications Magazine*, vol. 56, no. 7, pp. 36-41, July 2018.

[14] O. Quevedo-Teruel, M. Ebrahimpouri and M. Ng Mou Kehn, "Ultrawideband Metasurface Lenses Based on Off-Shifted Opposite Layers," in *IEEE Antennas and Wireless Propagation Letters*, vol. 15, pp. 484-487, Dec. 2016.

[15] S. Mueller *et al*., "Broad-band microwave characterization of liquid crystals using a temperature-controlled coaxial transmission line," in *IEEE Transactions on Microwave Theory and Techniques*, vol. 53, no. 6, pp. 1937-1945, June 2005.

[16] G. Valerio, A. Galli, D. R. Wilton and D. R. Jackson, “An enhanced integral-equation formulation for accurate analysis of frequency-selective structures,” in *International Journal of Microwave and Wireless Technologies*, vol. 4, no 3, pp. 365-372, 2012.